

PAPER • OPEN ACCESS

Comparative study of enzymatic and non-enzymatic detection of glucose using manganese ferrite nanoparticles

To cite this article: Monunith A *et al* 2020 *Mater. Res. Express* 7 094001

View the [article online](#) for updates and enhancements.



ECS The Electrochemical Society
Advancing solid state & electrochemical science & technology
2021 Virtual Education

Fundamentals of Electrochemistry:
Basic Theory and Kinetic Methods
Instructed by: **Dr. James Noël**
Sun, Sept 19 & Mon, Sept 20 at 12h–15h ET

Register early and save!

The advertisement features a photograph of an open book with its pages fanned out, resting on a wooden desk next to a laptop. In the background, there are three green chalkboards with white diagrams and chemical structures drawn on them.



PAPER

Comparative study of enzymatic and non-enzymatic detection of glucose using manganese ferrite nanoparticles

OPEN ACCESS

RECEIVED

28 March 2020

REVISED

17 August 2020

ACCEPTED FOR PUBLICATION

27 August 2020

PUBLISHED

4 September 2020

Original content from this work may be used under the terms of the [Creative Commons Attribution 4.0 licence](#).

Any further distribution of this work must maintain attribution to the author(s) and the title of the work, journal citation and DOI.

Monunith A¹, Arunima Rajan S^{1,2} and Niroj Kumar Sahu¹ ¹ Centre for Nanotechnology Research, Vellore Institute of Technology, Vellore-632014, India² School of Advanced Sciences, Vellore Institute of Technology, Vellore-632014, IndiaE-mail: nirojs@vit.ac.in**Keywords:** glucose oxidase, manganese ferrite, nanoparticles, glucose sensing, cyclic voltammetry, amperometrySupplementary material for this article is available [online](#)**Abstract**

The use of metal oxide nanoparticles for the development of cost-effective glucose biosensors has been receiving increased attention. Enzymatic and non-enzymatic glucose sensor using polyethylene glycol (PEG) grafted manganese ferrite (PEG-MnFe₂O₄) nanoparticles (NPs) modified onto a glassy carbon electrode (GCE) is reported in the present study. XRD and Raman studies confirmed the cubic spinel structure of MnFe₂O₄. The immobilization of glucose oxidase (GOx) on PEG-MnFe₂O₄ (GOx@PEG-MnFe₂O₄) was validated using FTIR and TGA. Sensing electrodes exhibited well-defined redox peaks in 0.1 M phosphate buffered saline (PBS) solution at pH 7.4 against the reference electrode Ag/AgCl. GOx@PEG-MnFe₂O₄/GCE displayed a sensitivity of 1.985 $\mu\text{A mM}^{-1} \text{cm}^{-2}$ in the linear range of 1 to 20 mM with a limit of detection (LOD) of 0.132 mM whereas non-enzymatic sensor exhibited a sensitivity of 1.044 $\mu\text{A mM}^{-1} \text{cm}^{-2}$ in the linear range of 1 to 10 mM with a LOD of 0.099 mM. The lower Michaelis constant (K_m^{app}) value indicates greater affinity towards glucose for the enzymatic sensor. GOx@PEG-MnFe₂O₄ revealed selectivity specifically for glucose over various interferants such as fructose, lactic acid, sucrose, uric acid and ascorbic acid. In addition, this enzymatic sensor demonstrated better reproducibility and lifetime.

1. Introduction

Diabetes mellitus commonly referred to as diabetes is one of the major health concerns affecting vast majority of the world population. As estimated by the International Diabetes Federation (IDF), one in every 10 people suffers from diabetes and approximately 463 million adults in the age group of 20 to 79 years are having diabetes [1]. Diabetes is a condition resulting from the lack of insulin in body which causes abnormally high blood-glucose concentration (hyperglycemia). Monitoring the glucose level is a critical factor for the treatment of diabetes as higher dosage of medicine can trigger glucose level to drop below the normal (hypoglycemia). Reusable type glucose sensors are not commercially available and the development of such reusable sensors can revolutionize the field. Many glucose sensors (both enzymatic and non-enzymatic) are being developed in which the enzymatic type makes use of an enzyme for direct reaction with glucose aiding for electron transfer while non-enzymatic sensors cause the direct oxidation of glucose.

Enzymatic electrochemical glucose sensors have been receiving immense attention for blood glucose detection due to its high sensitivity, selectivity and low limit of detection (LOD). Among the widely used enzymes, glucose oxidase (GOx) catalyses glucose oxidation in presence of oxygen to D-glucono-1,5-lactone which then hydrolyses to gluconic acid and hydrogen peroxide whereas the enzyme glucose dehydrogenase catalyses glucose to D-glucono-1,5-lactone [2]. GOx is considered as the gold standard for enzymatic glucose sensing owing to its high specificity to glucose. GOx is a homodimeric enzyme with flavin adenine dinucleotide (FAD) bound non-covalently to its active sites [2]. However, direct electron transfer between enzymes and electrode can lead to very less sensitivity. The activity of electrode can be enhanced by conjugating nanomaterials based on carbon [3–7], noble metals [8] along with their alloys [9–11], transition metals [12] and their oxides

[13, 14] or alloys [15] which will aid in the electron transfer as a mediator to the sensing electrode. In spite of the fact that enzymatic glucose sensors possess high selectivity and stability, their use is restricted due to poor enzymatic activity influenced by pH, humidity, thermal conditions and presence of chemicals which degrade the enzyme [8]. These drawbacks propelled extensive research in the field of non-enzymatic sensors, out of which transition metals and their alloys have been proven to be most effective with high selectivity and sensitivity [14], however, the associated high cost limits their usage. Lee *et al* reported the performance of enzymatic and nonenzymatic glucose sensors using nanostructured Au–Ni alloy. This work demonstrated the superior performance of the enzymatic glucose sensor with sensitivity of $1.302 \mu\text{A mM}^{-1}$ with LOD of $0.29 \mu\text{M}$ validating excellent selectivity, stability and linear range compared with non-enzymatic sensor with sensitivity $0.9601 \mu\text{A mM}^{-1}$ with LOD of $5.84 \mu\text{M}$ [16]. In a similar study, Mohapatra *et al.* investigated enzymatic and non-enzymatic glucose sensors using a carbon nano-onion modified sensor possessing a higher sensitivity for the enzymatic one with $26.5 \mu\text{A mM}^{-1} \text{cm}^{-2}$ with LOD of 0.21mM compared to the non-enzymatic with $21.6 \mu\text{A mM}^{-1} \text{cm}^{-2}$ with LOD of 0.09mM [3]. All these experimental investigations suggested the potential of NPs-based glucose bio-sensors for improving the sensing performance with high stability, sensitivity, selectivity and LOD.

Spinel ferrites have been reported to increase the electronic conductivity, structural stability and reversibility of the electrode material which can improve the performance of electrochemical sensing devices [17]. Manganese ferrite (MnFe_2O_4), one of the spinel ferrites, possesses beneficial properties such as enhanced electrical and magnetic properties with thermal and chemical stabilities, has been applied in various fields such as batteries [18], ferrofluids [19], catalysts [20] and biomedical applications [21, 22]. In the present study, MnFe_2O_4 has been chosen for glucose sensing owing to its excellent biocompatibility apart from the above-mentioned advantages. In order to improve the monodispersity and structural stability of the nanoparticles (NPs), conducting polymers such as polyethylene glycol (PEG), polyethylenimine (PEI), polyvinyl alcohol (PVA), polyaniline (PANI) are being extensively investigated for biosensing applications [23]. Polymers can act as coatings which provide electrostatic, steric, or electrosteric repulsive forces between magnetic nanoparticles (MNPs) preventing aggregation and promoting NPs dispersity as well as colloidal stability [24]. Monodispersity improves the electrical conductivity of NPs which is beneficial for sensing applications. Moreover, such polymers have been utilized for the construction of biosensors as well as supporting matrix for the electrochemical activity. PEG is one of the most explored polymers as stabilizing or coating agent for NPs [25–27]. This hydrophilic biocompatible conducting polymer has been approved by the Food and Drug Administration for various biomedical [28] and sensing applications [29, 30]. Several methods such as coprecipitation, hydrothermal, microemulsion, thermal decomposition, microwave-assisted etc have been introduced to synthesize MNPs [31, 32] Among the synthesis processes, hydrothermal method possesses the advantage of the formation of monodispersed, morphologically controlled and better crystalline natured MNPs [33–35].

In the present study, PEG grafted MnFe_2O_4 NPs via hydrothermal approach have been synthesized and tested towards glucose sensing. A comparative analysis for enzymatic and non-enzymatic glucose sensing has been reported. Here, PEG- MnFe_2O_4 NPs act as mediators for promoting electron transfer in enzymatic glucose sensor whereas direct oxidation reaction of glucose results for electron transfer in non-enzymatic glucose sensor. Finally, the results of two electrodes were compared to evaluate the better sensing performance.

2. Materials and methods

2.1. Materials

Glucose oxidase (GOx), D + glucose, manganese chloride tetrahydrate ($\text{MnCl}_2 \cdot 4\text{H}_2\text{O}$), iron chloride hexahydrate ($\text{FeCl}_3 \cdot 6\text{H}_2\text{O}$), ethylene glycol, hydrazine hydrate, polyethylene glycol (PEG)-4000, uric acid, L—ascorbic acid and nafion were purchased from Sigma-Aldrich. Sodium hydroxide (NaOH), ethanol ($\text{C}_2\text{H}_5\text{OH}$), potassium chloride (KCl), potassium ferricyanide ($\text{K}_3[\text{Fe}(\text{CN})_6]$), sucrose, D—fructose and lactic acid were purchased from SDFCL. 10X PBS (7.4 pH) was purchased from SRL. Deionised (DI) water was used throughout the experiments

2.2. Synthesis of MnFe_2O_4 NPs via hydrothermal method

$\text{MnCl}_2 \cdot 4\text{H}_2\text{O}$ and $\text{FeCl}_3 \cdot 6\text{H}_2\text{O}$ in 1:2 ratios dissolved in 50 ml of ethylene glycol were taken in a 100 ml teflon container. 1 g PEG dissolved in 5 ml ethylene glycol was then added to the above mixture. Upon complete dissolution, 5 ml of hydrazine hydrate was added to the above mixture and maintained the pH at 12. The whole solution was stirred for 1 h under nitrogen blanket and then transferred to a stainless-steel autoclave and kept in a furnace at 200°C for 24 h. Later, the synthesized material was washed with water and ethanol several times and separated using magnetic separation. The synthesized sample is labelled as PEG- MnFe_2O_4 .

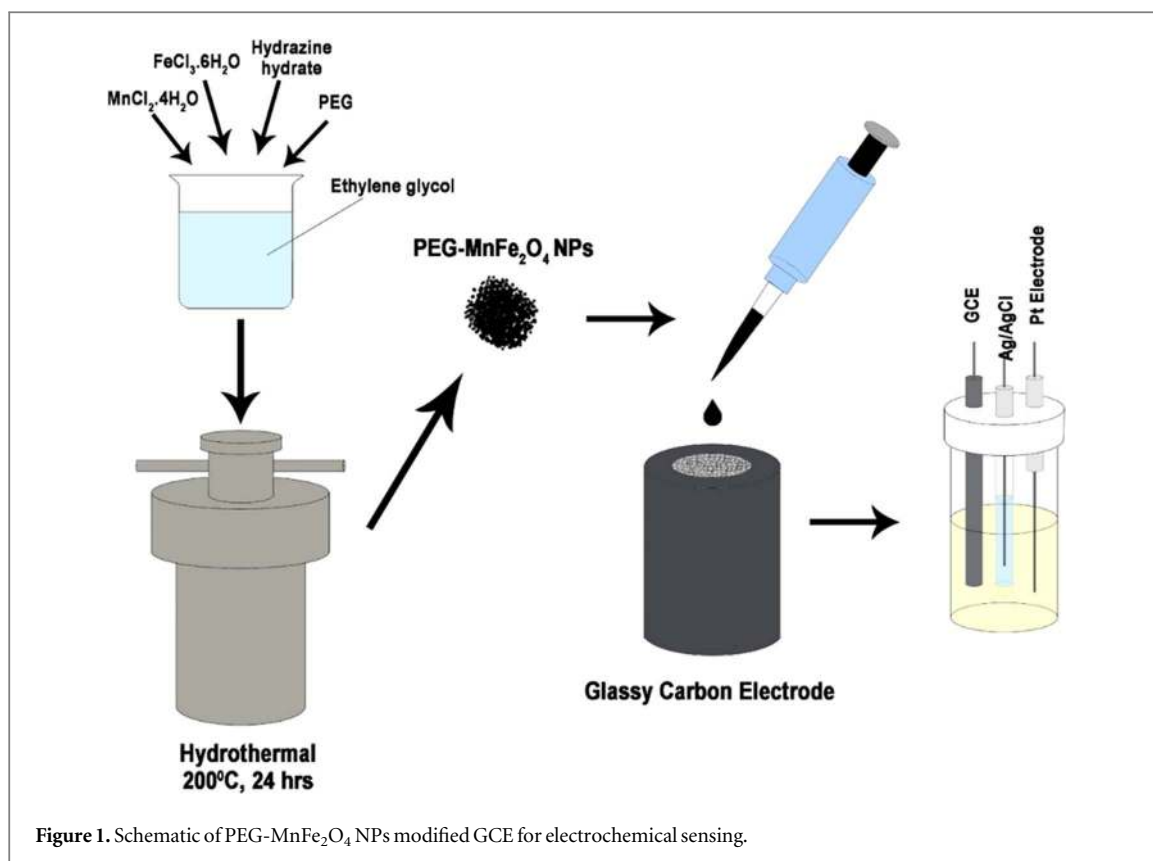


Figure 1. Schematic of PEG-MnFe₂O₄ NPs modified GCE for electrochemical sensing.

2.3. GOx immobilized MnFe₂O₄ modified GCE

Glassy carbon electrode (GCE) was first polished with 1.0 μ , 0.3 μ and 0.05 μ grade alumina powder and then wiped with DI water and ethanol. 5 μ l of the PEG-MnFe₂O₄ solution was dropped on to the GCE and kept for drying to obtain PEG-MnFe₂O₄/GCE. Later, 5 μ l of GOx was dropped on to the PEG-MnFe₂O₄/GCE followed by casting 5 μ l nafion on the surface of PEG-MnFe₂O₄/GCE to prevent the detachment of GOx during experimentation. GOx immobilized MnFe₂O₄ is labelled as GOx@PEG-MnFe₂O₄.

2.4. Electrochemical analysis

Electrochemical experiments were performed using a CHI660C electrochemical analyzer with 20 ml of 0.5 M KCl + 2 mM K₃[Fe(CN)₆] as supporting electrolyte. The cyclic voltammetry (CV) was carried out in the potential range from -0.8 to 0.8 V for the bare GCE, PEG-MnFe₂O₄/GCE and GOx@PEG-MnFe₂O₄/GCE at different scan rates of 10, 50 and 100 mV s⁻¹. CV for different glucose concentration ranging from 0–10 mM were carried out in an electrolyte of 0.1 M PBS at 7.4 pH. Differential pulse voltammetry (DPV) was also conducted at 10 mV increment for both the electrodes. Amperometric analysis was performed with the addition of glucose in an electrolyte of 0.1 M NaOH at -0.7057 V to -0.3730 V. The selectivity was further studied for enzymatic sensor by adding interferants such as fructose, lactic acid, sucrose, uric acid and ascorbic acid with the concentration of 10 mM. A schematic illustration of PEG-MnFe₂O₄ NPs modified GCE for electrochemical sensing is shown in figure 1.

2.5. Material characterizations

Phase and crystal structure of the NPs were characterised using x-ray Diffraction (XRD) recorded in Bruker D8 Advance equipment at $\lambda = 1.54$ Å from Cu K α radiation. Raman spectra providing information about the chemical bonding were recorded using a HORIBA Scientific system equipped with 532 nm laser source at 3.6 mW laser power. Surface functionalization and GOx loading was confirmed using Fourier transform Infrared (FTIR, IR Affinity-1 Spectrophotometer) spectroscopy. Thermogravimetric analysis (TGA) was performed for determining the thermal stability with the aid of a TGA, SDT Q600, TA Instruments by heating the sample from room temperature to 800 °C under nitrogen environment. Morphology was studied using FEI, Tecnai G2 F30 Field Emission Gun-Transmission Electron Microscope 300 kV (HR-TEM) and a FEI, Quanta 200 Field Emission Scanning Electron Microscope (FESEM). BET and BJH isotherms were used to investigate the pore size, pore volume distribution and specific surface area employing Quantachrome Nova Station 1000 instrument. CV, DPV and amperometric analysis of the NPs were measured in a three-electrode based CHI660C

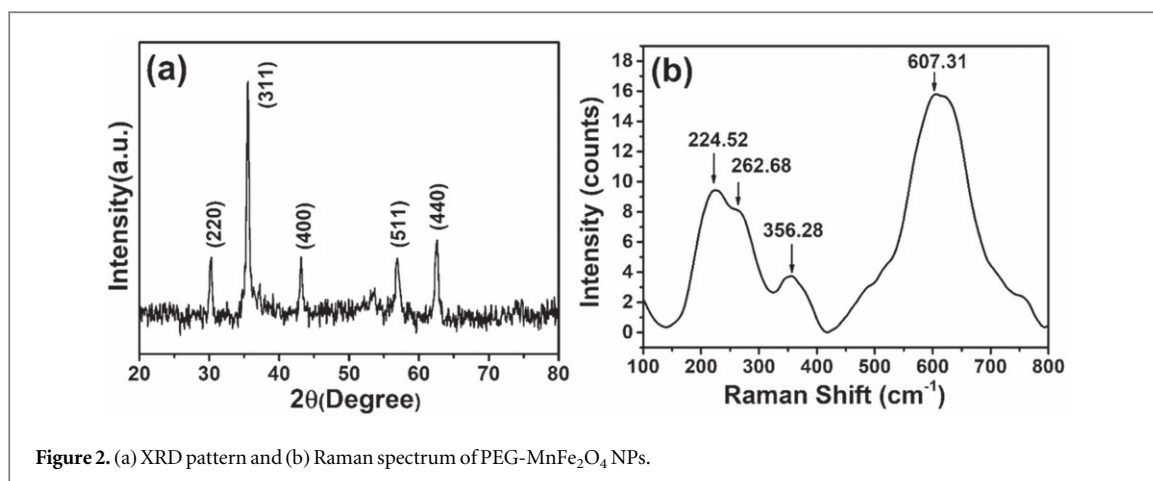


Figure 2. (a) XRD pattern and (b) Raman spectrum of PEG-MnFe₂O₄ NPs.

electrochemical workstation. GCE, Ag/AgCl and platinum were used as working, reference and counter electrodes respectively.

3. Results and discussions

3.1. Structural analysis

The XRD patterns, shown in figure 2(a) exhibit peaks corresponding to the cubic spinel manganese ferrite crystal structure (JCPDS No.073-1964). Major peaks at 2θ (degree) values of 30.29, 35.53, 43.13, 56.92, and 62.61° correspond to the planes (220), (311), (400), (511) and (440) respectively of MnFe₂O₄. Sharp peaks revealed the highly crystalline nature of the sample. No other impurity peaks have been detected. The average crystallite size of the NPs is calculated to be 21.23 ± 0.42 nm according to Debye–Scherrer equation based on full width half maximum of the major peak at 35.53°. The lattice parameter ‘a’ is estimated to be 8.37 Å using formula $a = d \times \sqrt{h^2 + k^2 + l^2}$ where h , k and l represents the miller indices of the major peak and d is the interplanar spacing. The calculated value is very close to the reported value in JCPDS No.073-1964 of MnFe₂O₄. PEG incorporation does not transform the crystal structure and phase of MnFe₂O₄.

3.2. Raman spectroscopy

Raman spectrum of PEG-MnFe₂O₄ NPs in the frequency range of 100–800 cm⁻¹ is shown in figure 2(b). Broad peaks observed at ~224, 262, 356 and 607 cm⁻¹ closely match to those reported value for MnFe₂O₄ [36]. A slight shift in the peaks towards lower wavelength can be observed which is ascribed to the longer chemical bond length of the molecule [37]. High frequency peak at ~607 cm⁻¹ belongs to the A_{1g} (Mn²⁺O) vibrational mode associated with the symmetric stretching of oxygen atoms along Mn–O bond at the tetrahedral site. Peaks observed at ~224, 262 and 356 cm⁻¹ correspond to the A_{1g}, E_g and T₁ modes respectively of Fe³⁺–O bond at the octahedral site [38]. No other impurity modes are observed revealing the pristine MnFe₂O₄ NPs.

3.3. FTIR analysis

FTIR spectrum of PEG-MnFe₂O₄ NPs in figure 3(a) displays two characteristic metal-oxygen bands at ~872 and 545 cm⁻¹ which can be assigned to Mn–O and Fe–O bonds at tetrahedral and octahedral sites respectively. Two bands observed at ~1420 cm⁻¹ and ~1633 cm⁻¹ correspond to the C–H bending and O–H stretching vibrations of PEG respectively [39]. A weak band at ~2950 cm⁻¹ corresponds to the asymmetric CH₂ bending vibration whereas a broad vibration band near ~3346 cm⁻¹ attributes to OH stretching vibrations of water molecules adsorbed on the surface of NPs [40]. These observed bands revealed the successful coating of PEG onto the surface of MnFe₂O₄ NPs. FTIR spectrum (in figure 3(b)) of bare GOx exhibits a broad absorption band at ~3280 cm⁻¹ corresponding to the N–H stretching and peaks observed at ~1639 cm⁻¹ and ~1531 cm⁻¹ correspond to the amide bands [41]. Specifically, band at ~1639 cm⁻¹ is observed due to the carbonyl (C=O) vibrations of peptide bonds whereas ~1531 cm⁻¹ is due to the N–H in-plane bending and C–N stretching modes of polypeptide chains of bare GOx. FTIR spectrum of GOx@PEG-MnFe₂O₄ shown in figure 3(c) exhibits similar peaks of PEG-MnFe₂O₄ and GOx confirming the successful coating of GOx on PEG-MnFe₂O₄. It is proposed that negatively charged nitrogen (N⁻) of NH₂ groups present in GOx effectively coordinates PEG-MnFe₂O₄ via physical adsorption resulting in GOx@PEG-MnFe₂O₄.

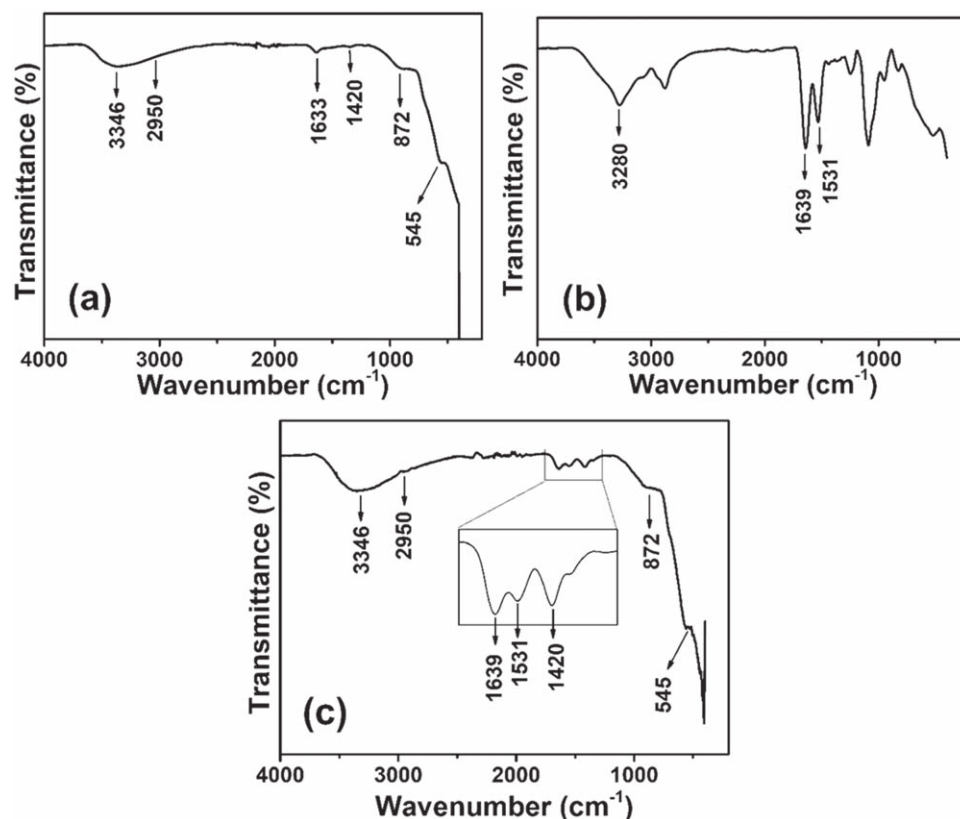


Figure 3. FTIR spectra of (a) PEG-MnFe₂O₄ NPs, (b) GOx and (c) GOx@PEG-MnFe₂O₄.

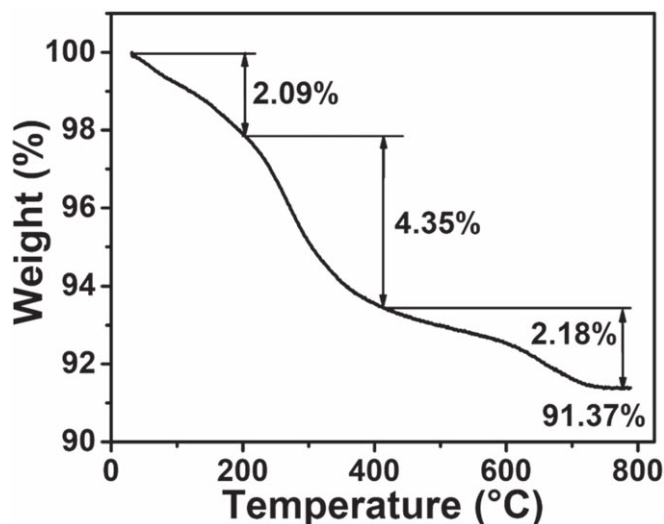


Figure 4. Weight versus temperature plot of GOx@PEG-MnFe₂O₄ NPs.

3.4. Thermal analysis (TGA)

TGA curve of GOx@PEG-MnFe₂O₄ NPs in figure 4 exhibits three significant weight losses. A gradual weight loss observed below 200 °C is due to the desorption of adsorbed water. Second significant weight loss observed in between 200–400 °C is attributed to the loss of GOx confirming the immobilization of GOx on the surface of PEG-MnFe₂O₄ NPs as weight loss due to GOx generally starts around 200 °C [42]. Third weight loss observed above 400 °C can be ascribed to the complete decomposition of PEG chemisorbed on the surface of MnFe₂O₄ NPs. A total weight loss of around 8.6% affirms improved thermal stability. Therefore, it is obvious that the immobilization of GOx on PEG-MnFe₂O₄ as well as binding of PEG on MnFe₂O₄ has been effectively accomplished.

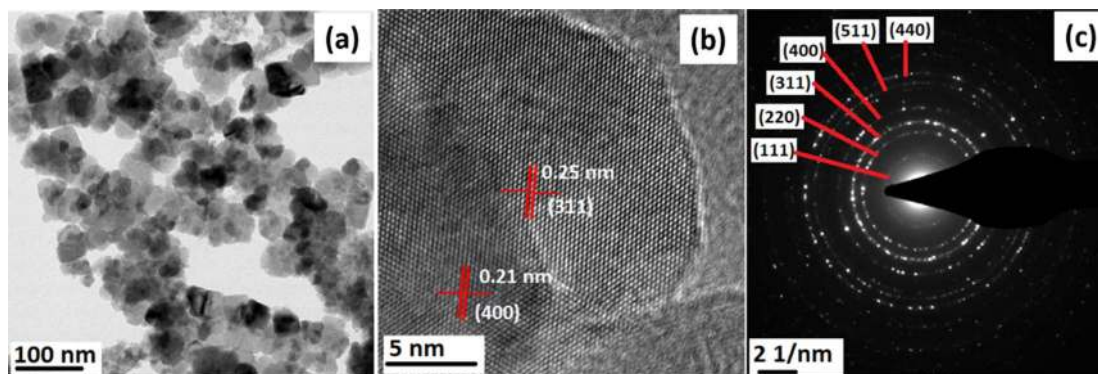


Figure 5. (a) HRTEM image, (b) lattice fringes and (c) SAED pattern of PEG-MnFe₂O₄ NPs.

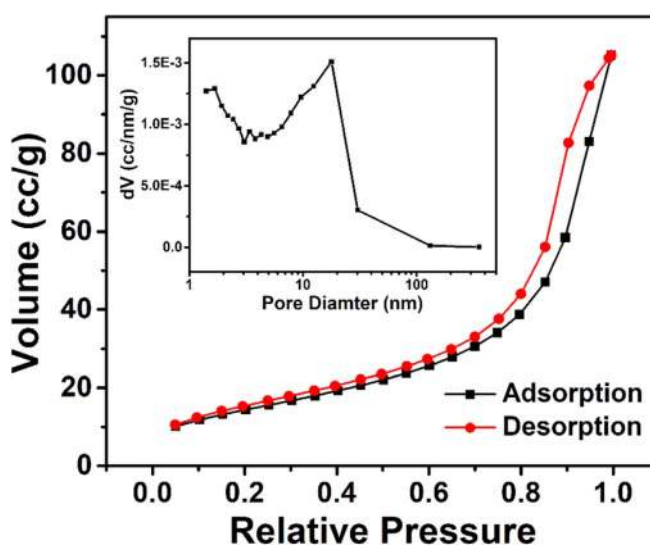


Figure 6. N₂ adsorption- desorption isotherms with pore size distribution (inset) of PEG-MnFe₂O₄ NPs.

3.5. Microstructural analysis

HRTEM micrograph of PEG-MnFe₂O₄ NPs in figure 5(a) exhibits an interconnected network of particles possessing a quasi-cubic shape with a dimension of $\sim 40.7 \pm 3.87$ nm. Figure 5(b) displays the lattice fringes which correspond to the (311) plane with an interplanar spacing of 0.25 nm and (400) plane with a spacing of 0.21 nm. Selected area electron diffraction (SAED) pattern in figure 5(c) matches with XRD data confirming the cubic spinel structure of MnFe₂O₄. Diffraction rings correspond to (111), (220), (311), (400), (511) and (440) planes with interplanar spacing of 0.49 nm, 0.31 nm, 0.25 nm, 0.21 nm, 0.16 nm and 0.15 nm respectively of MnFe₂O₄ (JCPDS card No. 73-1964). Moreover, from the FESEM micrographs (figure S1 is available online at stacks.iop.org/MRX/7/094001/mmedia), it has been confirmed that the individual NPs aggregate and form an interconnected structure resembling directional growth probably due to polymer coating and/or presence of ions like Fe³⁺ and Mn²⁺. According to the compacted morphology, it is expected that the immobilisation of GOx onto the surface of PEG-MnFe₂O₄ NPs is via physical adsorption rather than via pores.

3.6. BET analysis

The BET analysis (figure 6) suggests that PEG-MnFe₂O₄ NPs exhibit an average pore diameter of ~ 4.54 nm with a pore volume of 0.059 cc/g and a BET surface area of 52.71 m² g⁻¹. Though the exact dimensions of glucose oxidase are still uncertain, values for the dimeric structure fall within the mesoporous range ($7 \times 5.5 \times 8$ nm for the dimer) [43]. The immobilization of GOx occurs via pores when the size of the enzyme is comparable to the surface pores outside of NPs. Since the average pore size of the NPs is small compared to the dimensions of the enzyme, the immobilization of the GOx enzyme onto the surface of PEG-MnFe₂O₄ is assumed to be accrued not via pores rather than by physical adsorption through hydrogen bonding. This hypothesis is consistent with the reported literature [44].

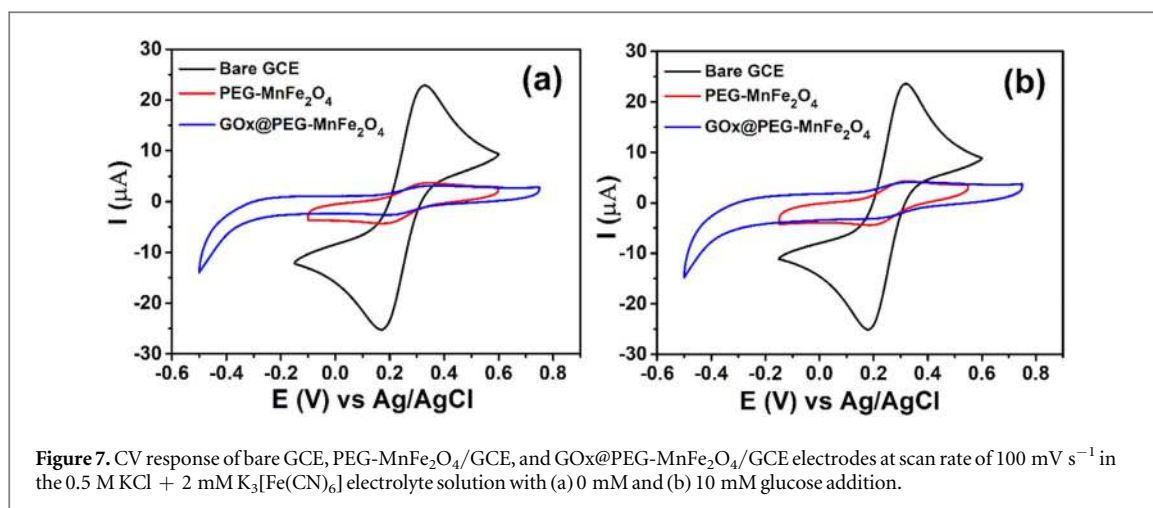


Figure 7. CV response of bare GCE, PEG-MnFe₂O₄/GCE, and GOx@PEG-MnFe₂O₄/GCE electrodes at scan rate of 100 mV s⁻¹ in the 0.5 M KCl + 2 mM K₃[Fe(CN)₆] electrolyte solution with (a) 0 mM and (b) 10 mM glucose addition.

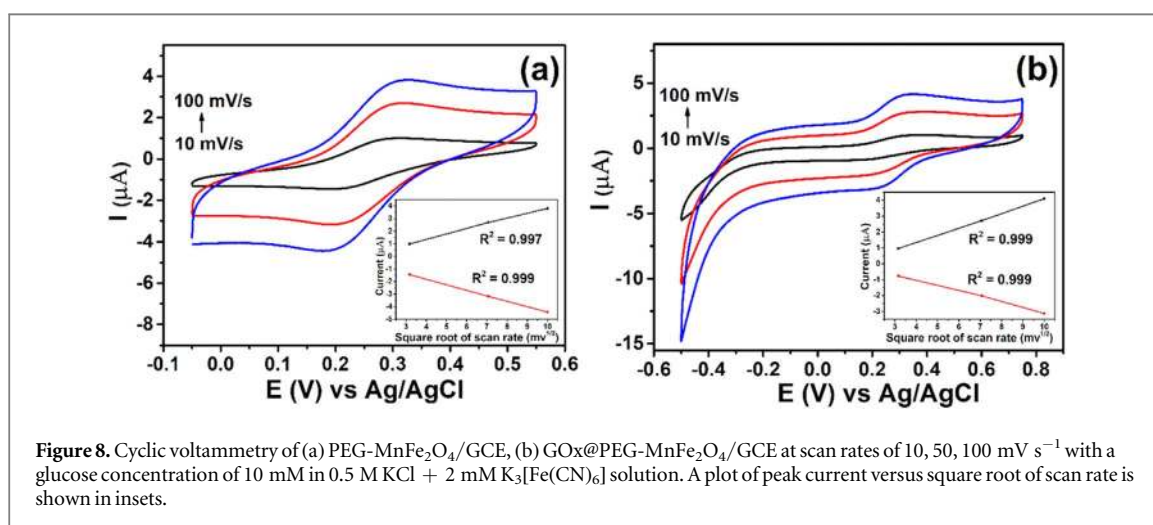


Figure 8. Cyclic voltammetry of (a) PEG-MnFe₂O₄/GCE, (b) GOx@PEG-MnFe₂O₄/GCE at scan rates of 10, 50, 100 mV s⁻¹ with a glucose concentration of 10 mM in 0.5 M KCl + 2 mM K₃[Fe(CN)₆] solution. A plot of peak current versus square root of scan rate is shown in insets.

3.7. Electrochemical study

3.7.1. Cyclic voltammetry (CV)

The electrocatalytic activities of PEG-MnFe₂O₄/GCE and GOx@PEG-MnFe₂O₄/GCE were studied using cyclic voltammetry. Figure 7 displays the CV of bare GCE, PEG-MnFe₂O₄/GCE and GOx@PEG-MnFe₂O₄/GCE in 0.5 M KCl + 2 mM K₃[Fe(CN)₆] electrolyte in presence and absence of glucose at a scan rate 100 mV s⁻¹. CV curve displays oxidation—reduction peaks for all the three systems confirming the occurrence of redox reaction due to the presence of Fe³⁺/Fe²⁺ in the ferricyanide solution. CV for GOx@PEG-MnFe₂O₄/GCE electrode exhibits the maximum current variation among others. GOx reduces flavin adenine dinucleotide (FAD) to FADH₂ which produces electrons and PEG-MnFe₂O₄ NPs promote the electron transfer as a mediator to the sensing electrode. However, the current values are lesser for PEG-MnFe₂O₄/GCE electrode due to the absence of a highly reactive material (GOx) causing for electron transfer.

Figure 8 shows the I–V curves of PEG-MnFe₂O₄/GCE and GOx@PEG-MnFe₂O₄/GCE with different scan rates of 10, 50 and 100 mV s⁻¹ for a glucose concentration of 10 mM. Increasing scan rate increases the anodic current (highest oxidation current) for both enzymatic and non-enzymatic sensor. Among these, higher oxidation current of 4.097 μA was observed for GOx@PEG-MnFe₂O₄/GCE than PEG-MnFe₂O₄/GCE (oxidation current is 3.81 μA) for the highest scan rate of 100 mV s⁻¹. This suggests that GOx@PEG-MnFe₂O₄/GCE shows better electrocatalytic activity towards glucose oxidation. It is evident that the anodic peak current increases linearly with square root of scan rate with high correlation coefficient R² (shown in inset of figures 8(a), (b)) indicating that the reaction is diffusion controlled according to Randles–Sevcik model [4, 45, 46]. In addition, the electron transfer process exhibited a quasi-reversible nature. The electro-active surface area for the GOx@PEG-MnFe₂O₄/GCE was determined using Randles–Sevcik equation:

$$I_p = 2.69 \times 10^5 AD^{1/2} N^{3/2} \gamma^{1/2} C$$

where I_p represents the maximum current in Ampere; γ , the scan rate is 100 mV s⁻¹; N , the electrons participating in the redox reaction which is 1 for the [Fe(CN)₆]^{4-/3-}; D , the diffusion coefficient calculated from

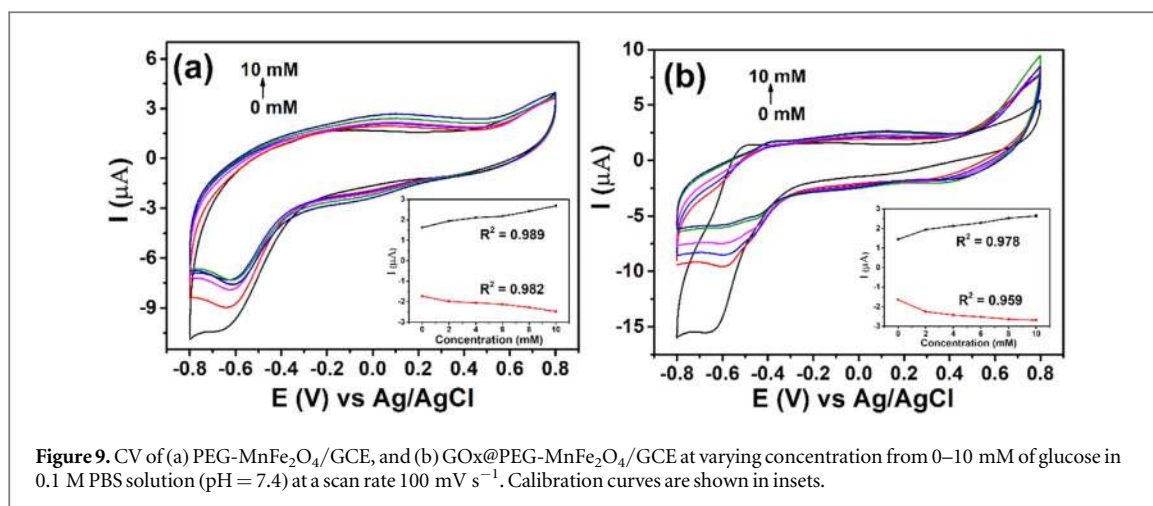
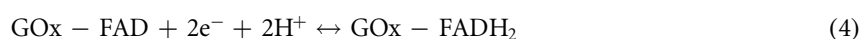
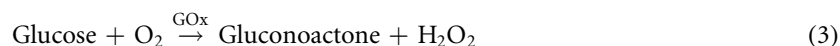
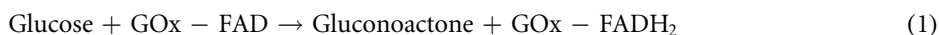


Figure 9. CV of (a) PEG-MnFe₂O₄/GCE, and (b) GOx@PEG-MnFe₂O₄/GCE at varying concentration from 0–10 mM of glucose in 0.1 M PBS solution (pH = 7.4) at a scan rate 100 mV s⁻¹. Calibration curves are shown in insets.

slope of current and square root of scan rate found to be $4.571 \times 10^{-7} \text{ cm}^2 \text{ s}^{-1}$ and C , concentration of analyte in the solution (mol cm^{-3}). The electro active surface area (A) is found to be 0.00712 cm^2 and 0.00697 cm^2 for GOx@PEG-MnFe₂O₄/GCE and PEG-MnFe₂O₄/GCE respectively. These results imply that electroactive surface area of both these electrodes seems to be similar evidencing improved conductivity.

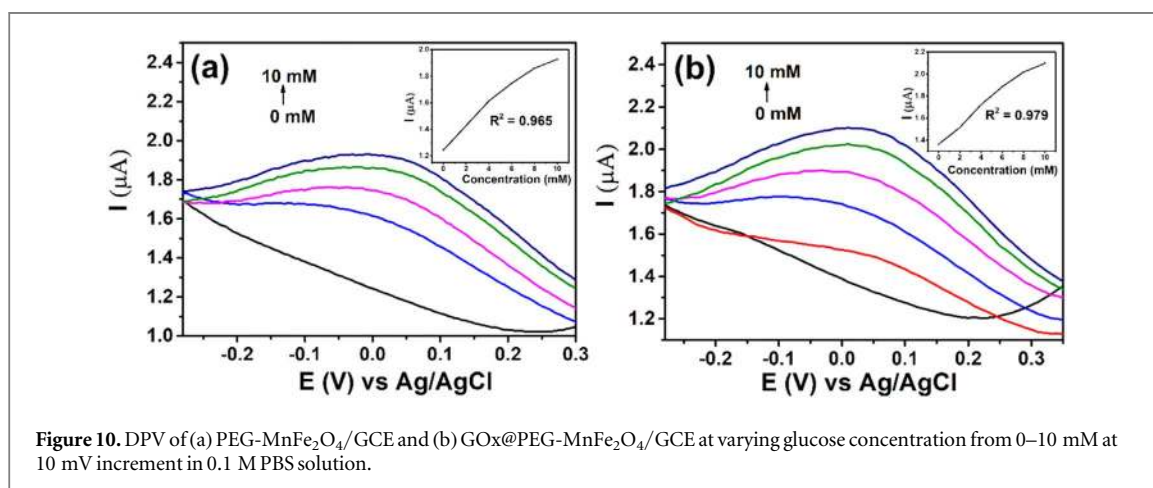
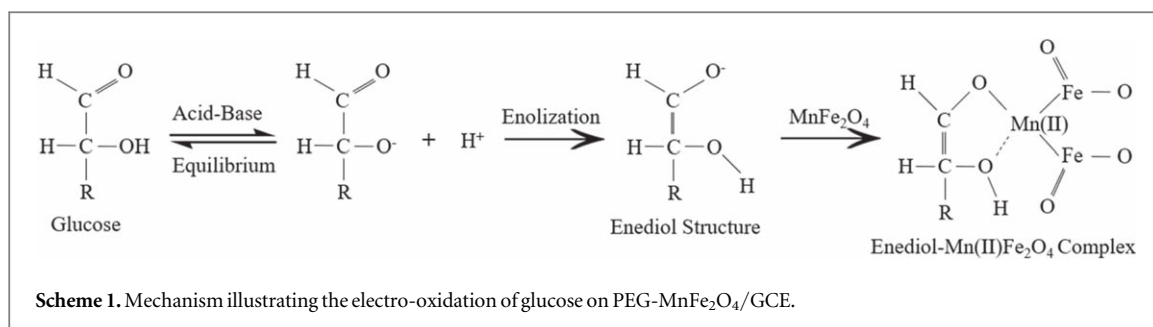
For determining the effective performance of the electrodes in physiological conditions, current response at varying glucose concentration of 0 to 10 mM and at a scan rate of 100 mV s⁻¹ using 0.1 M PBS as electrolyte was investigated. It is observed that both the electrodes exhibited electrocatalytic activity towards glucose oxidation in PBS solution. Figure 9(a) depicts the CV of PEG-MnFe₂O₄/GCE in which the anodic peak obtained at +0.1 V and the cathodic peak obtained at -0.1 V can be ascribed to the oxidation and reduction of glucose occurring due to the direct electron transfer from the NPs to the glucose in the solution. Similarly, anodic current increase with glucose concentration evident from figure 9(b) confirms that the glucose is catalysed by the enzyme GOx using oxygen to generate hydrogen peroxide [47]. The possible mechanism of glucose sensing is supported by the following redox reactions:



Oxidation and reduction peaks follow the reactions shown in equations (1) and (2) respectively. The overall redox reaction is presented in equation (3). In the absence of glucose, oxidation-reduction occurs due to the reversible reaction of GOx-FAD to GOx-FADH₂, given in equation (4). The anodic current increases with the glucose concentration and the oxidation peak value increases positively from 1.466 μA to 2.641 μA and 1.631 μA to 2.689 μA upon varying concentration from 0–10 mM in the enzymatic and non-enzymatic respectively. The higher electron transfer occurring in the enzymatic reaction leads to the maximum current variation in the enzymatic sensor compared to the non-enzymatic one. GOx reduces flavin adenine dinucleotide (FAD) to FADH₂ which produces electrons and PEG-MnFe₂O₄ NPs promote the electron transfer as a mediator to the sensing electrode. Higher affinity of PEG-MnFe₂O₄ NPs towards oxidation of the H₂O₂ produced during catalytic oxidation of glucose is also responsible for the better performance of enzymatic sensor than the non-enzymatic one as shown in equation (5). Furthermore, the O₂ produced in this reaction can help facilitate the reaction in equation (3). In the non-enzymatic sensor, the mechanism of electro-oxidation of glucose by PEG-MnFe₂O₄ NPs modified GCE is shown in scheme 1. Glucose in alkaline medium is susceptible to oxidation as glucose forms an enediol structure by losing a proton in the alkaline medium. This enediol structure forms an intermediate complex with the Mn²⁺ of PEG-MnFe₂O₄ leading to the electro-oxidation of glucose which is consistent with the reported literatures [48, 49]. The polymer PEG in this reaction acts as a conductive medium which does not affect the electro-oxidation of glucose whereas PEG in the enzymatic sensor aids for the physical adsorption of GOx. All peak current values (I_p) obtained is given in supplementary information tables S1–S3.

3.7.2. Differential pulse voltammetry (DPV)

DPV measurements of varying glucose concentrations in 0.1 M PBS are shown in figure 10. A regular interval pulse applied in system for DPV analysis provides smoother and better graphs. Similar to the above results,



oxidation and reduction peaks have exhibited a steady increase in current value as the concentration of glucose is increased. The calibration curve from DPV is also plotted for both the electrodes and the GOx@PEG-MnFe₂O₄/GCE has been found to possess a better response to the change in glucose concentration. This response is in accordance with the results obtained in CV, confirming that the enzymatic sensor has better response. Peak current values (I_p) obtained is given in supplementary information table S4.

3.7.3. Amperometric response

Figure 11(a) depicts the real time sensing capability of both the sensors. The response time for GOx@PEG-MnFe₂O₄/GCE is found to be 10 s and for PEG-MnFe₂O₄/GCE is 5 s. This time response indicates electron transfer from redox centre of the enzyme to PEG-MnFe₂O₄ NPs take a longer time as compared to direct redox reaction in PEG-MnFe₂O₄ NPs. The linear calibration curve for amperometric response is plotted in figure 11(b) which indicates that the current response increases linearly with the concentration of glucose for both the sensors. The sensitivity of GOx@PEG-MnFe₂O₄/GCE is determined to be 1.985 $\mu\text{A mM}^{-1}\text{cm}^{-2}$ in the linear range of 1 to 20 mM with a limit of detection of 0.132 mM from the slope of calibration curve. Similarly, the sensitivity of PEG-MnFe₂O₄/GCE is found to be 1.044 $\mu\text{A mM}^{-1}\text{cm}^{-2}$ in the range 1 to 10 mM and LOD of 0.099 mM.

Superior analytical performances in sensitivity and linear range are observed in case of the enzymatic glucose sensor. Glucose oxidase catalyses the oxidation of glucose in the presence of oxygen into D-glucono-1,5-lactone, which then hydrolyzes to gluconic acid and produces H₂O₂ according to the equations (1)–(3). Since this reaction produces H₂O₂ which could be further oxidized at the electrode, it leads to an increase in current from the enzymatic sensor. Hence, higher current and sensitivity observed for enzymatic sensor is due to the greater number of electrons involved. Higher affinity of PEG-MnFe₂O₄ NPs towards oxidation of the H₂O₂ produced during catalytic oxidation of glucose is also responsible for the better performance of enzymatic sensor [50, 51] than the non-enzymatic one. Direct glucose oxidation causes the non-enzymatic sensor to attain the saturation faster leading to the reduced linear range.

The curve displayed in figure S2 of the enzymatic sensor follows the Michaelis–Menten kinetics. The apparent Michaelis constant (K_m^{app}) and the maximum current (I_{max}) were obtained and used for analysing the response of the sensor towards glucose. The calibration curve follows a hyperbolic function $y = ax/(b + x)$, where the parameters a and b correspond to the I_{max} and K_m^{app} respectively [52, 53]. The values of I_{max} and K_m^{app} were found to be 3.5 μA and 18.5 mM respectively. The lower K_m^{app} value indicates that the enzymatic sensor has greater affinity towards glucose which is comparable to the value reported in literature [54].

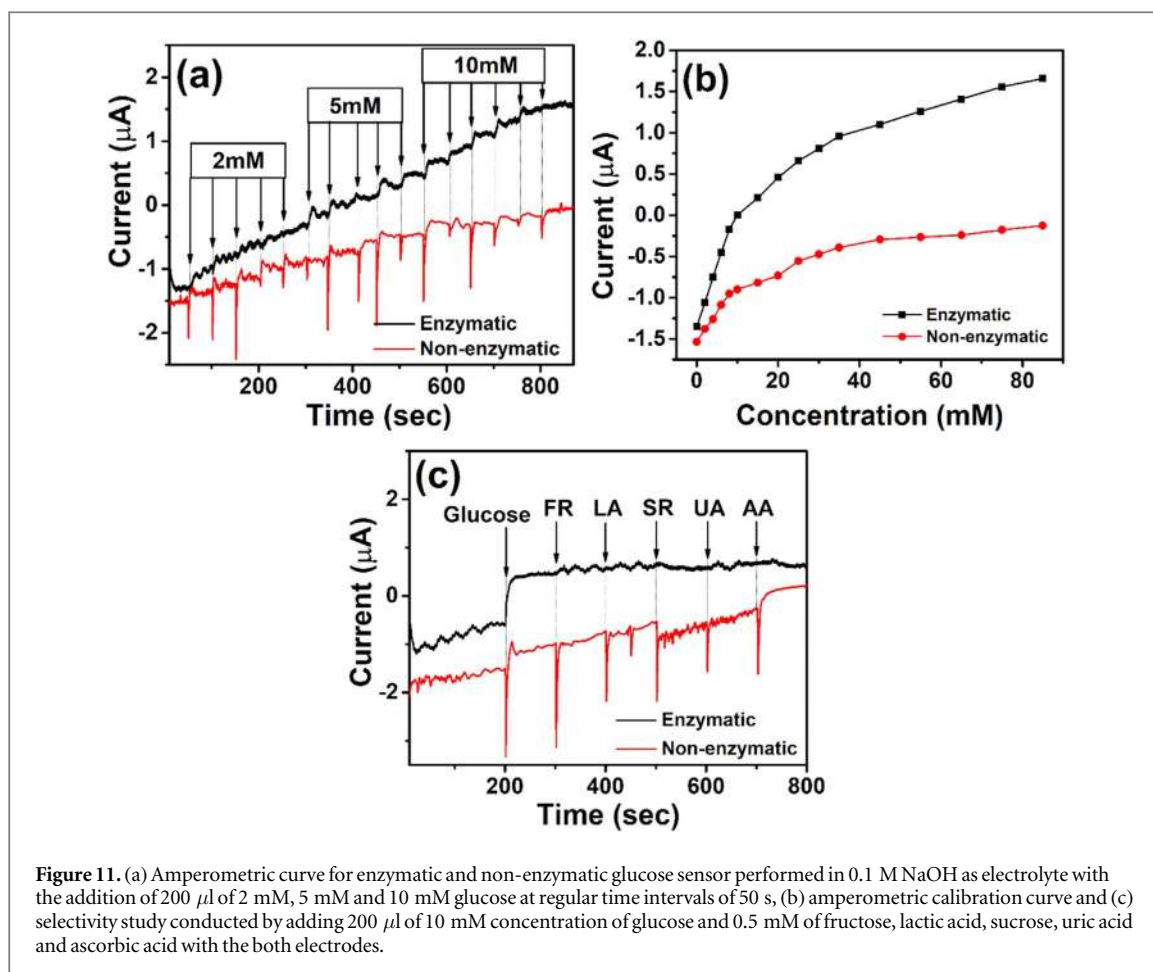


Figure 11. (a) Amperometric curve for enzymatic and non-enzymatic glucose sensor performed in 0.1 M NaOH as electrolyte with the addition of 200 μl of 2 mM, 5 mM and 10 mM glucose at regular time intervals of 50 s, (b) amperometric calibration curve and (c) selectivity study conducted by adding 200 μl of 10 mM concentration of glucose and 0.5 mM of fructose, lactic acid, sucrose, uric acid and ascorbic acid with the both electrodes.

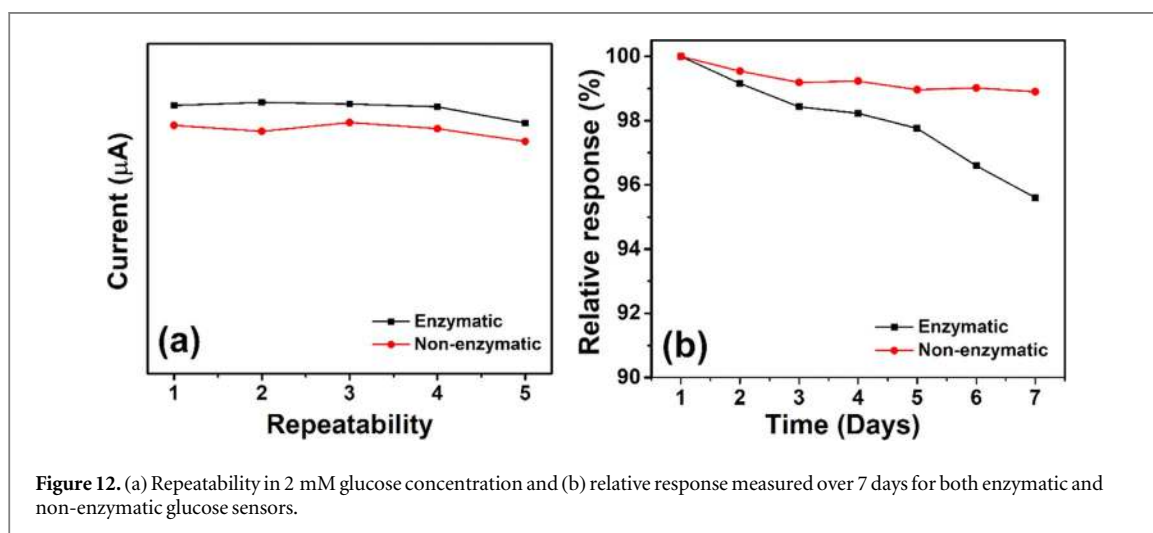


Figure 12. (a) Repeatability in 2 mM glucose concentration and (b) relative response measured over 7 days for both enzymatic and non-enzymatic glucose sensors.

The selectivity has been studied as shown in figure 11(c) using the interfering species such as fructose (FR), lactic acid (LA), sucrose (SR), uric acid (UA) and ascorbic acid (AA). As the normal level of glucose in physiological conditions is about 30 times more than these species [55], the selectivity study was conducted in 0.5 mM concentration of these interferents. Enzymatic sensor has exhibited higher selectivity to glucose within the potential range of -0.7057 V to -0.3730 V . Moreover, it exhibited a significant current response towards glucose after glucose addition compared to the negligible response with other interferents. In case of non-enzymatic sensor, selectivity study shows a noticeable current response towards glucose solution containing interference species when compared to enzymatic one. In summary, the enzymatic sensor exhibits high selectivity and specificity to glucose when compared with the non-enzymatic one. The obtained current values are given in supplementary information table S5.

3.7.4. Reproducibility and lifetime analysis

Reproducibility analysis was carried out 5 times with both enzymatic and non-enzymatic glucose sensors for 2 mM glucose concentration in PBS (pH 7.4) keeping the analysis parameters the same. The sensors exhibited reproducibility with a relative standard deviation (R.S.D) of 5.45% and 6.68% for enzymatic and nonenzymatic sensors respectively as shown in figure 12(a). The stability of both sensors was evaluated by monitoring the response current in the presence of 2 mM glucose over 7 days. The relative response of the sensor with respect to the initial value was found to be 95.6% for the enzymatic and 98.7% for the non-enzymatic sensor after 7 days as evident from figure 12(b). Both sensors exhibited substantial stability over the tested period of time owing to the strong binding of enzyme to the conductive polymer layer in the enzymatic sensor and the high stability of the PEG-MnFe₂O₄ NPs in the non-enzymatic sensor. The comparatively lower response of enzymatic sensor can be attributed to the slight amount of decomposition of GOx from the electrode surface. Hence, these results indicate that both electrodes displayed relatively stable reproducibility and lifetime.

4. Conclusion

PEG-MnFe₂O₄ NPs were successfully synthesised and immobilized with GOx for glucose sensing applications. A comparative study of PEG-MnFe₂O₄ NPs and GOx@PEG-MnFe₂O₄ has proved better activity for enzymatic sensor due to the presence of GOx which catalyse the glucose oxidation. GOx@PEG-MnFe₂O₄ (enzymatic sensor) has displayed 1.9 times higher sensitivity with twice the linear range when compared to PEG-MnFe₂O₄ (non-enzymatic sensor). The better performance exhibited by the enzymatic sensor is due to the electron transfer caused by the catalytic oxidation of glucose by GOx, which is facilitated by the PEG-MnFe₂O₄ NPs. Higher affinity of these NPs towards oxidation of the H₂O₂ generated during catalytic oxidation of glucose also contribute towards the enhanced performance. In addition, enzymatic sensor exhibits high selectivity and specificity to glucose within the applied potential range of -0.7057 V to -0.3730 V when compared with the non-enzymatic one. Further, the enzymatic sensor showed significant reproducibility and lifetime due to the stable enzyme immobilization onto the PEG-MnFe₂O₄ surface. This work emphasises the efficiency of PEG-MnFe₂O₄ NPs for glucose sensing applications.

Acknowledgments

The authors would like to gratefully acknowledge the DST-SERB (Project grant No. ECR/2016/000301) research grant for financially supporting the work.

ORCID iDs

Niroj Kumar Sahu  <https://orcid.org/0000-0002-0499-4108>

References

- [1] Saeedi P *et al* 2019 Global and regional diabetes prevalence estimates for 2019 and projections for 2030 and 2045: Results from the International Diabetes Federation Diabetes Atlas *Diabetes Research and Clinical Practice* **157** 107843
- [2] Ferri S, Kojima K and Sode K 2011 Review of glucose oxidases and glucose dehydrogenases: a bird's eye view of glucose sensing enzymes *J. Diabetes Sci. Technol.* **5** 1068–76
- [3] Mohapatra J, Ananthoju B, Nair V, Mitra A, Bahadur D, Medhekar N V and Aslam M 2018 Enzymatic and non-enzymatic electrochemical glucose sensor based on carbon nano-onions *Appl. Surf. Sci.* **442** 332–41
- [4] Zhu Z, Song W, Burugapalli K, Moussy F, Li Y L and Zhong X H 2010 Nano-yarn carbon nanotube fiber based enzymatic glucose biosensor *Nanotechnology* **21** 165501
- [5] Chung R, Wang A and Peng S 2017 An enzymatic glucose sensor composed of carbon-coated nano tin sulfide *Nanomaterials*. **7** 39
- [6] Zhang W, Chen J and Jiang L 2010 A highly sensitive nonenzymatic glucose sensor based on NiO-modified multi-walled carbon nanotubes *Microchim. Acta* **168** 259–65
- [7] Li L and Zhang W 2008 Preparation of carbon nanotubes supported platinum nanoparticles by an organic colloidal process for nonenzymatic glucose sensing *Microchim. Acta* **163** 305–11
- [8] Topçu Sulak M, Gökdoğan Ö, Gülce A and Gülce H 2006 Amperometric glucose biosensor based on gold-deposited polyvinylferrocene film on Pt electrode *Biosens. Bioelectron.* **21** 1719–26
- [9] Yehezkeili I, Tel-Vered O, Raichlin R and Willner S 2011 Nano-engineered flavin-dependent glucose dehydrogenase/gold nanoparticle-modified electrodes for glucose sensing and biofuel cell *ACS Nano*. **5** 2385–91
- [10] Shim J H, Cha A, Lee Y and Lee C 2011 Nonenzymatic amperometric glucose sensor based on nanoporous gold/ruthenium electrode *Electroanalysis*. **23** 2057–62
- [11] Madhura T R, Kumar G G and Ramaraj R 2019 Gold nanoparticles decorated silicate sol-gel matrix embedded reduced graphene oxide and manganese ferrite nanocomposite- materials- modified electrode for glucose sensor application *J. Chem. Sci.* **131** 1–11
- [12] Sun F, Li L and Liu P 2011 Nonenzymatic electrochemical glucose sensor based on novel copper film *Electroanalysis*. **23** 395–401

- [13] Wang G, Wei Y and Zhang W 2010 Enzyme-free amperometric sensing of glucose using Cu–CuO nanowire composites *Microchim. Acta* **168** 87–92
- [14] Zhang X, Zhang Z, Liao Q, Liu S, Kang Z and Zhang Y 2016 Nonenzymatic glucose sensor based on *in situ* reduction of Ni/NiO-graphene nanocomposite *Sensors (Switzerland)*. **16** 1–10
- [15] Gong X, Gu Y, Zhang F, Liu Z, Li Y and Chen G 2019 High-performance non-enzymatic glucose sensors based on CoNiCu alloy nanotubes arrays prepared by electrodeposition *Front. Mater.* **6** 3
- [16] Lee D S, Kim W C, Gurudatt K B, Hussain N G, Choi K K, Park C S and Shim Y B 2019 Comparison of enzymatic and non-enzymatic glucose sensors based on hierarchical Au–Ni alloy with conductive polymer *Biosens. Bioelectron.* **130** 48–54
- [17] Nagamuthu S, Vijayakumar S, Lee S-H and Ryu K-S 2016 Hybrid supercapacitor devices based on MnCo₂O₄ as the positive electrode and FeMn₂O₄ as the negative electrode *Appl. Surf. Sci.* **390** 202–8
- [18] Zhang Z, Wang Y, Tan Q, Zhong Z and Su F 2013 Facile solvothermal synthesis of mesoporous manganese ferrite (MnFe₂O₄) microspheres as anode materials for lithium-ion batteries *J. Colloid Interface Sci.* **398** 185–92
- [19] Arulmurugan R, Vaidyanathan G, Sendhilnathan S and Jayadevan B 2006 Mn–Zn ferrite nanoparticles for ferrofluid preparation: study on thermal–magnetic properties *J. Magn. Magn. Mater.* **298** 83–94
- [20] Valdés-Sol[\] is T, Valle-Vigón P, Álvarez S, Marbán G and Fuertes A B 2007 Manganese ferrite nanoparticles synthesized through a nanocasting route as a highly active Fenton catalyst *Catal. Commun.* **8** 2037–42
- [21] Khan A, Rajan S A, Chandunika R K and Sahu N K 2019 Magneto-plasmonic stimulated breast cancer nanomedicine *External Field and Radiation Stimulated Breast Cancer Nanotheranostics* (IOP: IOPscience) **5** 5-1–5-27
- [22] Chandunika R K, Vijayaraghavan R and Sahu N K 2020 Magnetic hyperthermia application of MnFe₂O₄ nanostructures processed through solvents with the varying boiling point *Mater. Res. Express* **7** 1–10
- [23] Wang X and Uchiyama S 2013 Polymers for biosensors construction *State of the Art in Biosensors—General Aspects* (London: IntechOpen) **3** 67–84.
- [24] Zare Y 2016 Study of nanoparticles aggregation/agglomeration in polymer particulate nanocomposites by mechanical properties *Compos. Part A Appl. Sci. Manuf.* **84** 158–64
- [25] Rani B, Punnikoti S and Sahu N K 2018 Polyol asserted hydrothermal synthesis of SnO₂ nanoparticles for the fast adsorption and photocatalytic degradation of methylene blue cationic dye *New J. Chem.* **42** 943–54
- [26] Rajan S A, Sharma M and Sahu N K 2019 Water-to-PEG variation: morphology and hyperthermic behaviour of iron oxide *J. Supercond. Nov. Magn.* **33** 1603–9
- [27] Chen Z and Gao L 2007 Synthesis and magnetic properties of CoFe₂O₄ nanoparticles by using PEG as surfactant additive *Mater. Sci. Eng. B* **141** 82–6
- [28] Molineux G 2003 Pegylation: engineering improved biopharmaceuticals for oncology *Pharmacother. J. Hum. Pharmacol. Drug Ther.* **23** 3S–8S
- [29] Salariya K, Umar A, Kansal S K and Mehta S K 2017 Rapidly synthesized polyethylene glycol coated cadmium sulphide (CdS) nanoparticles as potential scaffold for highly sensitive and selective lethal cyanide ion sensor *Sensors Actuators B Chem.* **241** 276–84
- [30] Loiseau A, Asila V, Boitel-Aullen G, Lam M, Salmain M and Boujday S 2019 Silver-based plasmonic nanoparticles for and their use in biosensing *Biosensors*. **9** 78
- [31] Tatarchuk T, Bououdina M, Vijaya J J and Kennedy L J 2016 Spinel ferrite nanoparticles: synthesis, crystal structure, properties, and perspective applications *Int. Conf. Nanotechnol. Nanomater.* **305**–25
- [32] Rani B and Sahu N K 2020 Electrochemical properties of CoFe₂O₄ nanoparticles and its rGO composite for supercapacitor *Diam. Relat. Mater.* **108** 107978
- [33] Giri S, Samanta S, Maji S, Ganguli S and Bhaumik A 2005 Magnetic properties of α -Fe₂O₃ nanoparticle synthesized by a new hydrothermal method *J. Magn. Magn. Mater.* **285** 296–302
- [34] Rajan A and Sahu N K 2020 Inductive calorimetric assessment of iron oxide nano-octahedrons for magnetic fluid hyperthermia *Colloids Surfaces A Physicochem. Eng. Asp.* **603** 125210
- [35] Aparna M L, Grace A N, Sathyanarayanan P and Sahu N K 2018 A comparative study on the supercapacitive behaviour of solvothermally prepared metal ferrite (MFe₂O₄, M = Fe, Co, Ni, Mn, Cu, Zn) nanoassemblies *J. Alloys Compd.* **745** 385–95
- [36] Wang M, Ding W, Zhao Z, Wu X, Li S, Yue F and Liu J P 2015 Microstructure and magnetic properties of MFe₂O₄ (M = Co, Ni, and Mn) ferrite nanocrystals prepared using colloid mill and hydrothermal method *J. Appl. Phys.* **117** 6–10
- [37] Yu Q, Guan P, Qin D, Golden G and Wallace P M 2008 Inverted size-dependence of surface-enhanced Raman scattering on gold nanohole and nanodisk arrays *Nano Lett.* **8** 1923–8
- [38] Chamritski I and Burns G 2005 Infrared- And raman-active phonons of magnetite, maghemite, and hematite: a computer simulation and spectroscopic study *J. Phys. Chem. B* **109** 4965–8
- [39] Shah S A, Majeed A, Rashid K and Awan S U 2013 PEG-coated folic acid-modified superparamagnetic MnFe₂O₄ nanoparticles for hyperthermia therapy and drug delivery *Mater. Chem. Phys.* **138** 703–8
- [40] García-Jimeno S and Estelrich J 2013 Ferrofluid based on polyethylene glycol-coated iron oxide nanoparticles: characterization and properties *Colloids Surfaces A Physicochem. Eng. Asp.* **420** 74–81
- [41] Baghayeri M 2015 Glucose sensing by a glassy carbon electrode modified with glucose oxidase and a magnetic polymeric nanocomposite *RSC Adv.* **5** 18267–74
- [42] Sharma K P, Zhang Y, Thomas M R, Brogan A P S, Perriman A W and Mann S 2014 Self-organization of glucose oxidase-polymer surfactant nanoconstructs in solvent-free soft solids and liquids *J. Phys. Chem. B* **118** 11573–80
- [43] Ania C O, Gomis-Berenguer A, Dentzer J and Vix-Guterl C 2018 Nanoconfinement of glucose oxidase on mesoporous carbon electrodes with tunable pore sizes *J. Electroanal. Chem.* **808** 372–9
- [44] Jesionowski T, Zdzarta J and Krajewska B 2014 Enzyme immobilization by adsorption: a review *Adsorption* **20** 801–21
- [45] Hrapovic S, Liu Y, Male K B and Luong J H T 2004 Electrochemical biosensing platforms using platinum nanoparticles and carbon nanotubes *Anal. Chem.* **76** 1083–8
- [46] Allen L R F and Bard J 2000 *Electrochemical Methods: Fundamentals and Applications* 2nd edn (New York: Wiley) 978-0-471-04372-0
- [47] Zhang Y, Chen D, Ma X, Yang W, Li T, Dai D and Zhang B 2019 Direct electrochemistry of glucose oxidase based on one step electrodeposition of reduced graphene oxide incorporating polymerized L-lysine and its application in glucose sensing *Mater. Sci. Eng. C* **104** 109880
- [48] Shahnava Z, Lorestani F, Alias Y and Woi P M 2014 Polypyrrole–ZnFe₂O₄ magnetic nano-composite with core–shell structure for glucose sensing *Appl. Surf. Sci.* **317** 622–9
- [49] Qian L, Mao J, Tian X, Yuan H and Xiao D 2013 *In situ* synthesis of CuS nanotubes on Cu electrode for sensitive nonenzymatic glucose sensor *Sensors Actuators B Chem.* **176** 952–9

- [50] Li M, Xiong Y, Liu X, Bo X, Zhang Y, Han C and Guo L 2015 Facile synthesis of electrospun MFe_2O_4 ($M = Co, Ni, Cu, Mn$) spinel nanofibers with excellent electrocatalytic properties for oxygen evolution and hydrogen peroxide reduction *Nanoscale*. **7** 8920–30
- [51] Wu H, Wang J, Kang X, Wang C, Wang D, Liu J, Aksay I A and Lin Y 2009 Glucose biosensor based on immobilization of glucose oxidase in platinum nanoparticles/graphene/chitosan nanocomposite film *Talanta* **80** 403–6
- [52] Ramanavičius A, Kaušaitė A and Ramanavičienė A 2005 Polypyrrole-coated glucose oxidase nanoparticles for biosensor design *Sensors Actuators B Chem.* **111** 532–9
- [53] Anusha J R, Raj C J, Cho B-B, Fleming A T, Yu K-H and Kim B C 2015 Amperometric glucose biosensor based on glucose oxidase immobilized over chitosan nanoparticles from gladius of *Uroteuthis duvaucei* *Sensors Actuators B Chem.* **215** 536–43
- [54] Chen X, Jia J and Dong S 2003 Organically modified sol-gel/chitosan composite based glucose biosensor *Electroanal. An Int. J. Devoted to Fundam. Pract. Asp. Electroanal.* **15** 608–12
- [55] Zhang P, Zhang L, Zhao G and Feng F 2012 A highly sensitive nonenzymatic glucose sensor based on CuO nanowires *Microchim. Acta* **176** 411–7